

# 1 Genomic loci influence patterns of structural covariance in the human brain

## 2 Supporting Information

3  
4 Junhao Wen<sup>1,2\*</sup>, Ilya M. Nasrallah<sup>2,3</sup>, Ahmed Abdulkadir<sup>2</sup>, Theodore D. Satterthwaite<sup>2,4</sup>, Zhijian Yang<sup>2</sup>,  
5 Guray Erus<sup>2</sup>, Timothy Robert-Fitzgerald<sup>5</sup>, Ashish Singh<sup>2</sup>, Aristeidis Sotiras<sup>6</sup>, Aleix Boquet-Pujadas<sup>7</sup>,  
6 Elizabeth Mamourian<sup>2</sup>, Jimit Doshi<sup>2</sup>, Yuhan Cui<sup>2</sup>, Dhivya Srinivasan<sup>2</sup>, Ioanna Skampardoni<sup>2</sup>, Jiong  
7 Chen<sup>2</sup>, Gyujuon Hwang<sup>2</sup>, Mark Bergman<sup>2</sup>, Jingxuan Bao<sup>8</sup>, Yogasudha Veturi<sup>9</sup>, Zhen Zhou<sup>2</sup>, Shu Yang<sup>8</sup>,  
8 Paola Dazzan<sup>10</sup>, Rene S. Kahn<sup>11</sup>, Hugo G. Schnack<sup>12</sup>, Marcus V. Zanetti<sup>13</sup>, Eva Meisenzahl<sup>14</sup>, Geraldo F.  
9 Busatto<sup>13</sup>, Benedicto Crespo-Facorro<sup>15</sup>, Christos Pantelis<sup>16</sup>, Stephen J. Wood<sup>17</sup>, Chuanjun Zhuo<sup>18</sup>, Russell  
10 T. Shinohara<sup>2,5</sup>, Ruben C. Gur<sup>4</sup>, Raquel E. Gur<sup>4</sup>, Nikolaos Koutsouleris<sup>19</sup>, Daniel H. Wolf<sup>2,4</sup>, Andrew J.  
11 Saykin<sup>20</sup>, Marylyn D. Ritchie<sup>9</sup>, Li Shen<sup>8</sup>, Paul M. Thompson<sup>21</sup>, Olivier Colliot<sup>22</sup>, Katharina Wittfeld<sup>23</sup>,  
12 Hans J. Grabe<sup>23</sup>, Duygu Tosun<sup>24</sup>, Murat Bilgel<sup>25</sup>, Yang An<sup>25</sup>, Daniel S. Marcus<sup>26</sup>, Pamela LaMontagne<sup>26</sup>,  
13 Susan R. Heckbert<sup>27</sup>, Thomas R. Austin<sup>27</sup>, Lenore J. Launer<sup>28</sup>, Mark Espeland<sup>29</sup>, Colin L Masters<sup>30</sup>, Paul  
14 Maruff<sup>30</sup>, Jurgen Fripp<sup>31</sup>, Sterling C. Johnson<sup>32</sup>, John C. Morris<sup>33</sup>, Marilyn S. Albert<sup>34</sup>, R. Nick Bryan<sup>3</sup>,  
15 Susan M. Resnick<sup>25</sup>, Yong Fan<sup>2</sup>, Mohamad Habes<sup>35</sup>, David Wolk<sup>2,36</sup>, Haochang Shou<sup>2,5</sup>, and Christos  
16 Davatzikos<sup>2\*</sup>

17  
18 <sup>1</sup>Laboratory of AI and Biomedical Science (LABS), Stevens Neuroimaging and Informatics Institute, Keck School of  
19 Medicine of USC, University of Southern California, Los Angeles, California, USA.

20 <sup>2</sup>Artificial Intelligence in Biomedical Imaging Laboratory (AIBIL), Center for Biomedical Image Computing and  
21 Analytics, Perelman School of Medicine, University of Pennsylvania, Philadelphia, USA.

22 <sup>3</sup>Department of Radiology, University of Pennsylvania, Philadelphia, USA.

23 <sup>4</sup>Department of Psychiatry, Perelman School of Medicine, University of Pennsylvania, Philadelphia, USA

24 <sup>5</sup>Penn Statistics in Imaging and Visualization Center, Department of Biostatistics, Epidemiology, and Informatics,  
25 Perelman School of Medicine, University of Pennsylvania, Philadelphia, USA

26 <sup>6</sup>Department of Radiology and Institute for Informatics, Washington University School of Medicine, St. Louis, USA

27 <sup>7</sup>Biomedical Imaging Group, EPFL, Lausanne, Switzerland

28 <sup>8</sup>Department of Biostatistics, Epidemiology and Informatics University of Pennsylvania Perelman School of Medicine,  
29 Philadelphia, USA

30 <sup>9</sup>Department of Genetics and Institute for Biomedical Informatics, Perelman School of Medicine, University of  
31 Pennsylvania, Philadelphia, PA, USA

32 <sup>10</sup>Department of Psychological Medicine, Institute of Psychiatry, Psychology and Neuroscience, King's College  
33 London, London, UK

34 <sup>11</sup>Department of Psychiatry, Icahn School of Medicine at Mount Sinai, New York, USA

35 <sup>12</sup>Department of Psychiatry, University Medical Center Utrecht, Utrecht, Netherlands

36 <sup>13</sup>Institute of Psychiatry, Faculty of Medicine, University of São Paulo, São Paulo, Brazil

37 <sup>14</sup>Department of Psychiatry and Psychotherapy, HHU Düsseldorf, Germany

38 <sup>15</sup>Hospital Universitario Virgen del Rocío, University of Sevilla-IBIS; IDIVAL-CIBERSAM, Sevilla, Spain

39 <sup>16</sup>Melbourne Neuropsychiatry Centre, Department of Psychiatry, University of Melbourne and Melbourne Health,  
40 Carlton South, Australia

41 <sup>17</sup>Orygen and the Centre for Youth Mental Health, University of Melbourne; and the School of Psychology,  
42 University of Birmingham, UK

43 <sup>18</sup>Key Laboratory of Real Time Tracing of Brain Circuits in Psychiatry and Neurology (RTBCPN-Lab), Nankai  
44 University Affiliated Tianjin Fourth Center Hospital; Department of Psychiatry, Tianjin Medical University, Tianjin,  
45 China

46 <sup>19</sup>Department of Psychiatry and Psychotherapy, Ludwig-Maximilian University, Munich, Germany

47 <sup>20</sup>Radiology and Imaging Sciences, Center for Neuroimaging, Department of Radiology and Imaging Sciences,  
48 Indiana Alzheimer's Disease Research Center and the Melvin and Bren Simon Cancer Center, Indiana University  
49 School of Medicine, Indianapolis

50 <sup>21</sup>Imaging Genetics Center, Mark and Mary Stevens Neuroimaging and Informatics Institute, Keck School of  
51 Medicine of USC, University of Southern California, Marina del Rey, California

52 <sup>22</sup>Sorbonne Université, Institut du Cerveau - Paris Brain Institute - ICM, CNRS, Inria, Inserm, AP-HP, Hôpital de la  
53 Pitié Salpêtrière, F-75013, Paris, France

54 <sup>23</sup>Department of Psychiatry and Psychotherapy, German Center for Neurodegenerative Diseases (DZNE), University  
55 Medicine Greifswald, Germany  
56 <sup>24</sup>Department of Radiology and Biomedical Imaging, University of California, San Francisco, CA, USA  
57 <sup>25</sup>Laboratory of Behavioral Neuroscience, National Institute on Aging, NIH, USA  
58 <sup>26</sup>Department of Radiology, Washington University School of Medicine, St. Louis, Missouri, USA  
59 <sup>27</sup>Cardiovascular Health Research Unit and Department of Epidemiology, University of Washington, Seattle, WA,  
60 USA  
61 <sup>28</sup>Neuroepidemiology Section, Intramural Research Program, National Institute on Aging, Bethesda, Maryland, USA  
62 <sup>29</sup>Sticht Center for Healthy Aging and Alzheimer's Prevention, Wake Forest School of Medicine, Winston-Salem,  
63 North Carolina, USA  
64 <sup>30</sup>Florey Institute of Neuroscience and Mental Health, The University of Melbourne, Parkville, VIC, Australia  
65 <sup>31</sup>CSIRO Health and Biosecurity, Australian e-Health Research Centre CSIRO, Brisbane, Queensland, Australia  
66 <sup>32</sup>Wisconsin Alzheimer's Institute, University of Wisconsin School of Medicine and Public Health, Madison,  
67 Wisconsin, USA  
68 <sup>33</sup>Knight Alzheimer Disease Research Center, Washington University in St. Louis, St. Louis, MO, USA  
69 <sup>34</sup>Department of Neurology, Johns Hopkins University School of Medicine, USA  
70 <sup>35</sup>Glenn Biggs Institute for Alzheimer's & Neurodegenerative Diseases, University of Texas Health Science Center at  
71 San Antonio, San Antonio, USA  
72 <sup>36</sup>Department of Neurology and Penn Memory Center, University of Pennsylvania, Philadelphia, USA  
73  
74 \*Corresponding authors:  
75 Junhao Wen, Ph.D. – [junhaowe@usc.edu](mailto:junhaowe@usc.edu)  
76 2025 Zonal Ave, Los Angeles, CA 90033, United States  
77 Christos Davatzikos, Ph.D. – [Christos.Davatzikos@penndmedicine.upenn.edu](mailto:Christos.Davatzikos@penndmedicine.upenn.edu)  
78 3700 Hamilton Walk, 7th Floor, Philadelphia, PA 19104, United States  
79

80 eText 1: Sensitivity check analysis for the GWAS using PSC C32\_1  
81 eText 2: Institutional Review Board (IRB) statement  
82 eText 3: The four datasets and populations defined in this study  
83 eMethod 1: Empirical validation of sopNMF  
84 eMethod 2: Reproducibility index  
85 eMethod 3: Inter-site image harmonization  
86 eMethod 4: Quality check of the image processing pipeline  
87 eMethod 5 Definition of the index, candidate, independent significant, and SNP and  
88 genomic locus  
89 eMethod 6 Cross-validation procedure for PAML  
90 eFigure 1: Comparison between opNMF and sopNMF  
91 eFigure 2: Reproducibility of the sopNMF brain parcellation  
92 eFigure 3: Scatter plot for the  $h^2$  estimates from the discovery and replication sets  
93 eFigure 4: Sensitivity check for the GWAS results using the discovery set in UKBB  
94 eFigure 5: Machine learning performance for disease classification and age prediction  
95 eFigure 6: Annotation of MUSE PSCs to MuSIC PSCs based on the overlap index  
96 eFigure 7: Summary statistics of the multi-scale PSCs of MuSIC  
97 eTable 1: Study cohort characteristics  
98 eTable 2: Clinical phenotypes and diagnoses used in machine learning classification  
99 eTable 3: Comparison of variants identified via MuSIC with other studies  
100 eTable 4: Classification balanced accuracy for disease classification and effect size of these  
101 imaging signatures  
102 eTable 5: 119 MUSE gray matter regions of interest  
103 eAlgorithm 1: Algorithm for sopNMF  
104

105 **eText 1: Sensitivity check analysis for the GWAS using PSC C32\_1**

106 We used the GWAS results (233 significant SNPs in 5 genomic loci) of the first PSC in C32  
107 (C32\_1) from the UKBB discovery set to demonstrate this.

108 We replicated all the 233 significant SNPs in 5 genomic loci both at the nominal level ( $-\log_{10}[\text{p-value}] > 1.31$ ), and the Bonferroni corrected p-value threshold ( $-\log_{10}[\text{p-value}] > 3.67$ )  
109 using the combined discovery and replication sets ( $N=33,541$ ) (**SI eFigure 4b**), the 20,438  
110 participants with all ancestries in the discovery set (**SI eFigure 4c**), and the 16,743 participants  
111 in the discovery set with four additional imaging-related covariates (3 parameters for the brain  
112 position in the lateral, longitudinal, and transverse directions, and 1 parameter for the head  
113 motion from fMRI) (**SI eFigure 4d**). While replicating the results in 2386 participants with non-  
114 European ancestries, we only replicated 41 SNPs (17.6%), passing the nominal significant  
115 threshold (**SI eFigure 4e**). Finally, only 14 SNPs (6.4%) were replicated when replicating the  
116 results using 1481 whole-genome sequencing (WGS) data from ADNI consolidated by the  
117 AI4AD consortium<sup>16</sup> (**SI eFigure 4f**). The low replication rates in other ancestries and  
118 independent disease-specific populations are expected due to population stratification, disease-  
119 specific effects, and reduced sample sizes. This further emphasizes the urge to enrich and  
120 diversify genetic research with non-European ancestries and disease-specific populations.  
121

122

123 **eText 2: Institutional Review Board (IRB) statement**

124 All individual studies were approved by their local corresponding Institutional Review Boards  
125 (IRB). The iSTAGING and PHENOM consortia consolidated all individual imaging and clinical  
126 data; imputed genotype data were directly downloaded from the UKBB website. Data from the  
127 UKBB for this project pertains to application 35148. For iSTAGING, the IRB at the University  
128 of Pennsylvania (protocol number: 825722) reviewed the research proposal on August 31<sup>st</sup>, 2016,  
129 and updated it on August 31<sup>st</sup>, 2022. No human subjects were recruited or scanned. Existing de-  
130 identified data will be used in this mega-analysis study pooling data from 17 studies: BLSA,  
131 ADNI1, ADNI2, ADNI3, ACCORD-MIND, LookAhead, SPRINT, CARDIA, MESA, SHIP,  
132 BIOCARD, WRAP, Penn-ADC, WHIMS-MRI, AIBL, OASIS, UKBB, MESA, HANDLS. For  
133 PHENOM, the IRB at the University of Pennsylvania (protocol number: 828077) reviewed the  
134 research proposal on August 19<sup>th</sup>, 2017. No human subjects were recruited or scanned. Existing  
135 de-identified data will be used in this meta-analysis study pooling data from 10 studies at Penn,  
136 Ludwick-Maximmilian University of Munich, Kings College-London, University of Utrecht,  
137 University of Melbourne, University of Cantabria, University of Sao Paolo, Xijing Hospital  
138 Shaanxi, Tianjin Anning Hospital, and Institute of Mental Health Peking University.  
139

140 **eText 3: The four datasets and populations defined in this study**

141 We defined four populations or data sets per analysis across the paper: *i) discovery set, ii)*  
142 *replication set, iii) training population, and iv) comparison population* (refer to **SI eText 2** for  
143 details).

- 144 • Discovery set: It consists of a multi-disease and lifespan population that includes  
145 participants from all 12 studies ( $N=32,440$ ). Note that this population does not contain  
146 the entire UKBB population but only our first download (July 2017,  $N=21,305$ ).
- 147 • Replication set: We held 18,259 participants from the UKBB dataset to replicate the  
148 GWAS results. We took these data from our second download of the UKBB dataset  
149 (November 2021,  $N=18,259$ ).
- 150 • Training population: We randomly drew 250 patients (PT), including AD, MCI, SCZ,  
151 ASD, MDD, HTN (hypertension), DM (diabetes mellitus), and 250 healthy controls  
152 (CN) per decade from the discovery set, ensuring that the PT and CN groups have  
153 similar sex, study and age distributions. The resulting set of 4000 imaging data was used  
154 to generate the MuSIC atlas with the sopNMF algorithm. The rationale is to maximize  
155 variability across a balanced sample of multiple diseases or risk conditions, age, and  
156 study protocols rather than overfit the entire data by including all images in training.
- 157 • Comparison population: To validate sopNMF compared to the original opNMF  
158 algorithm, we randomly subsampled 800 participants from the training population (100  
159 per decade for balanced CN and PT). For this scale of sample size, opNMF can load all  
160 images into memory for batch learning.<sup>1</sup>

161

162 **eMethod 1: Empirical validation of sopNMF.**

163 For the empirical validation of sopNMF, the comparison population (**Method 1** in the main  
164 manuscript) was used so that the machine's memory could be sufficient to read the entire data for  
165 opNMF. For sopNMF, different choices of batch size (i.e., BS=32, 64, 128, and 256) were  
166 tested. We hypothesized that sopNMF could approximate the optima of opNMF during  
167 optimization, i.e., resulting in similar parts-based representation, training loss, and sparsity.  
168 TensorboardX was embedded into the sopNMF framework to monitor the training process  
169 dynamically. All experiments were performed on an Ubuntu machine with a maximum RAM of  
170 32 GB and 8 CPUs. The predefined maximum number of epochs for all experiments is 50,000,  
171 and the tolerance of early stopping criteria is 100 epochs based on the training loss.

172 We qualitatively compared the extracted PSCs and quantitatively for the training loss, the  
173 sparsity of the component matrix  $W$ , and the memory consumption for  $C=20$  (number of PSCs).  
174 The 20 PSCs were spatially consistent between opNMF and sopNMF, despite that some regions  
175 were decomposed into different PSCs (i.e., the white ellipse in **eFig. 1A**). For the training loss,  
176 opNMF obtained the lowest loss ( $1.103 \times 10^6$ ), and the loss of sopNMF were  $1.107 \times 10^6$ ,  $1.108$   
177  $\times 10^6$ ,  $1.111 \times 10^6$  and  $1.210 \times 10^6$  for BS =256, 128, 64, and 32, respectively (**eFig. 1D**). For the  
178 sparsity of the component matrix, all models obtained comparable results (sparsity  $\approx 0.83$ , **eFig.**  
179 **1E**). The estimated memory consumptions during the training process were 28.65, 4.02, 3.81,  
180 2.60, 1.47 GB for opNMF and sopNMF (BS =256, 128, 64, and 32), respectively  
181 (**Fig. e1F**).

182

183 **eMethod 2: Reproducibility index.**

184 We proposed a reproducibility index (RI) to test the reproducibility of sopNMF for brain

185 parcellation:

- 186 • We used the Hungarian match algorithm<sup>2</sup> to match the pairs of PSCs between two splits  
187 under the specific condition that maximizes the similarity (i.e., minimizes the cost of  
188 workers/jobs in its original formulation).
- 189 • For each pair of PSCs, we calculated the inner product of the vectors ( $R^d$ ), referred to as  
190 RI. This index takes values between [0, 1], with higher values indicating higher  
191 reproducibility.
- 192 • For each scale  $C$ , we presented the mean/standard deviation of the RIs for all PSCs.

193

194

195



196 **eMethod 3: Inter-site image harmonization**

197 We used an extensively validated statistical harmonization approach, i.e., ComBat-GAM,<sup>3</sup> to  
198 harmonize the extracted multi-scale PSCs. This method estimates the variability in volumetric  
199 measures due to differences in site/cohort-specific imaging protocols based on variances observed  
200 within and across control groups while preserving normal variances due to age, sex, and  
201 intracranial volume (ICV) differences. The model was initially trained on the discovery set and  
202 then applied to the replication set.

203

204 **eMethod 4: Quality check of the image processing pipeline.**

205 Raw T1-weighted MRIs were first quality checked (QC) for motion, image artifacts, or restricted  
206 field-of-view. Another QC was performed: First, the images were examined by manually  
207 evaluating for pipeline failures (e.g., poor brain extraction, tissue segmentation, and registration  
208 errors). Furthermore, a second step automatically flagged images based on outlying values of  
209 quantified metrics (i.e., PSC values); those flagged images were re-evaluated.

210

211 **eMethod 5: Definition of the index, candidate, independent significant, and lead SNP and**  
212 **genomic locus.**

213 *Index SNP*

214 They are defined as SNPs with a p-value threshold  $\leq 5e-8$  (*clump-p1*) from GWAS summary  
215 statistics.

216 *Independent significant SNP*

217 They are defined as the index SNPs, which are independent of each other (not in linkage  
218 disequilibrium) with  $r^2 \leq 0.6$  (*clump-r2*) within 250 kilobases (non-overlapping, *clump-kb*) away  
219 from each other.

220 *Lead SNP and genomic loci*

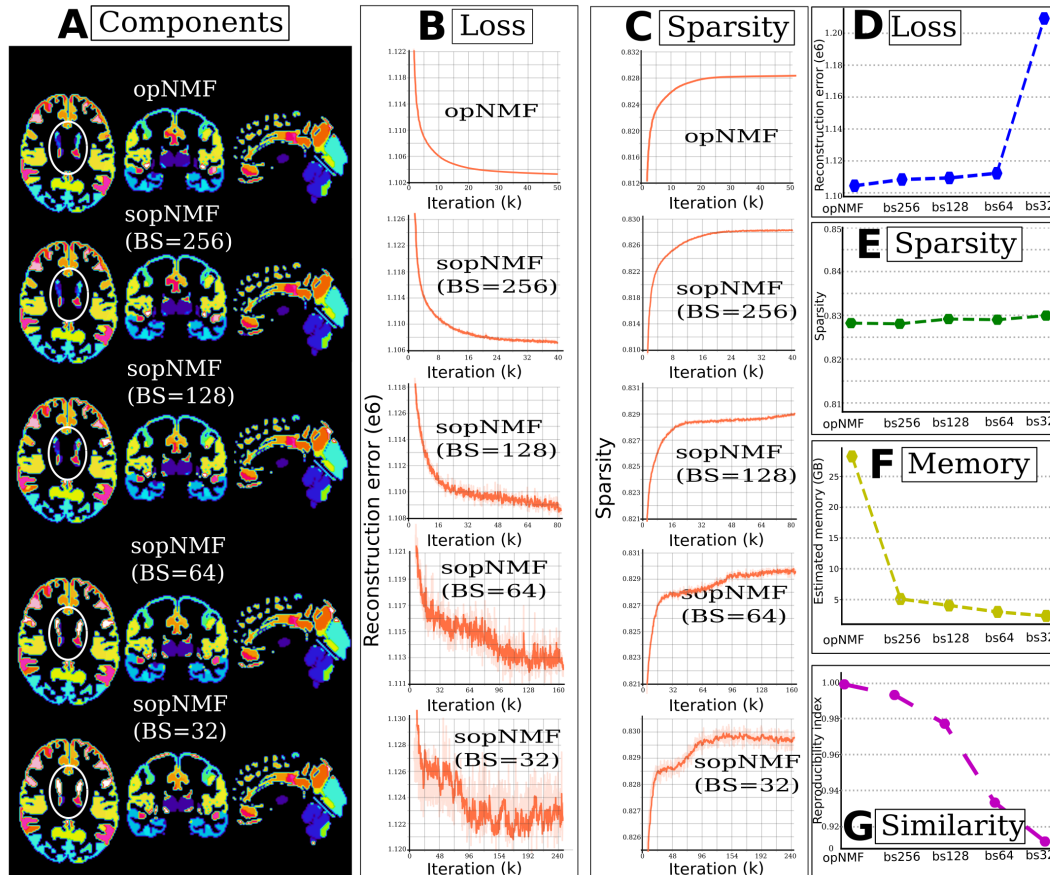
221 They are defined as the independent significant SNPs, which are independent of each other with  
222 a more stringent  $r^2 \leq 0.1$  (*clump-r2*) within 250 kilobases (non-overlapping, *clump-kb*) away  
223 from each other. Each of these clumps is defined as a *genomic locus*.

224 *Candidate SNP*

225 With each genomic locus, candidate SNPs are defined as the SNPs whose association p-values  
226 are smaller than 0.05 (*clump-p2*). The definitions followed instructions from FUMA<sup>4</sup> and Plink<sup>5</sup>  
227 software.

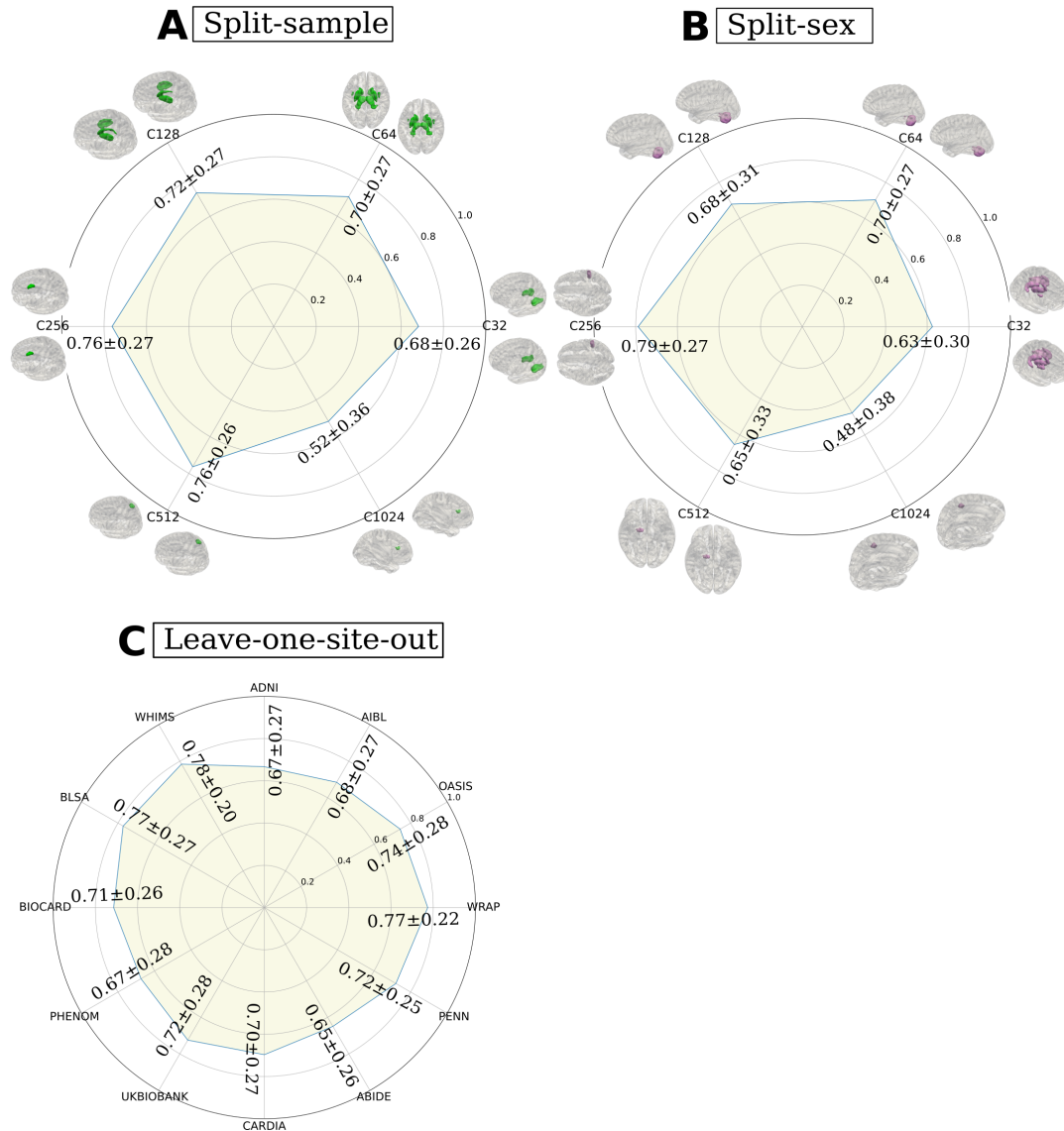
228 **eMethod 6: Cross-validation procedure for PAML.**

229 Nested cross-validation was adopted for all tasks following the good-practice guidelines  
230 proposed in our previous works<sup>6-8</sup>. In particular, an outer loop was used to evaluate the task  
231 performance (250 repetitions of random hold-out splits with 80% of data for training). In  
232 contrast, an inner loop focused on tuning the hyperparameters (10-fold splits). We computed the  
233 balanced accuracy (BA) to evaluate the classification tasks. We calculated the effect size  
234 (Cohen's  $d$ ) and p-value for each SPARE index to quantify its discriminative power.  
235

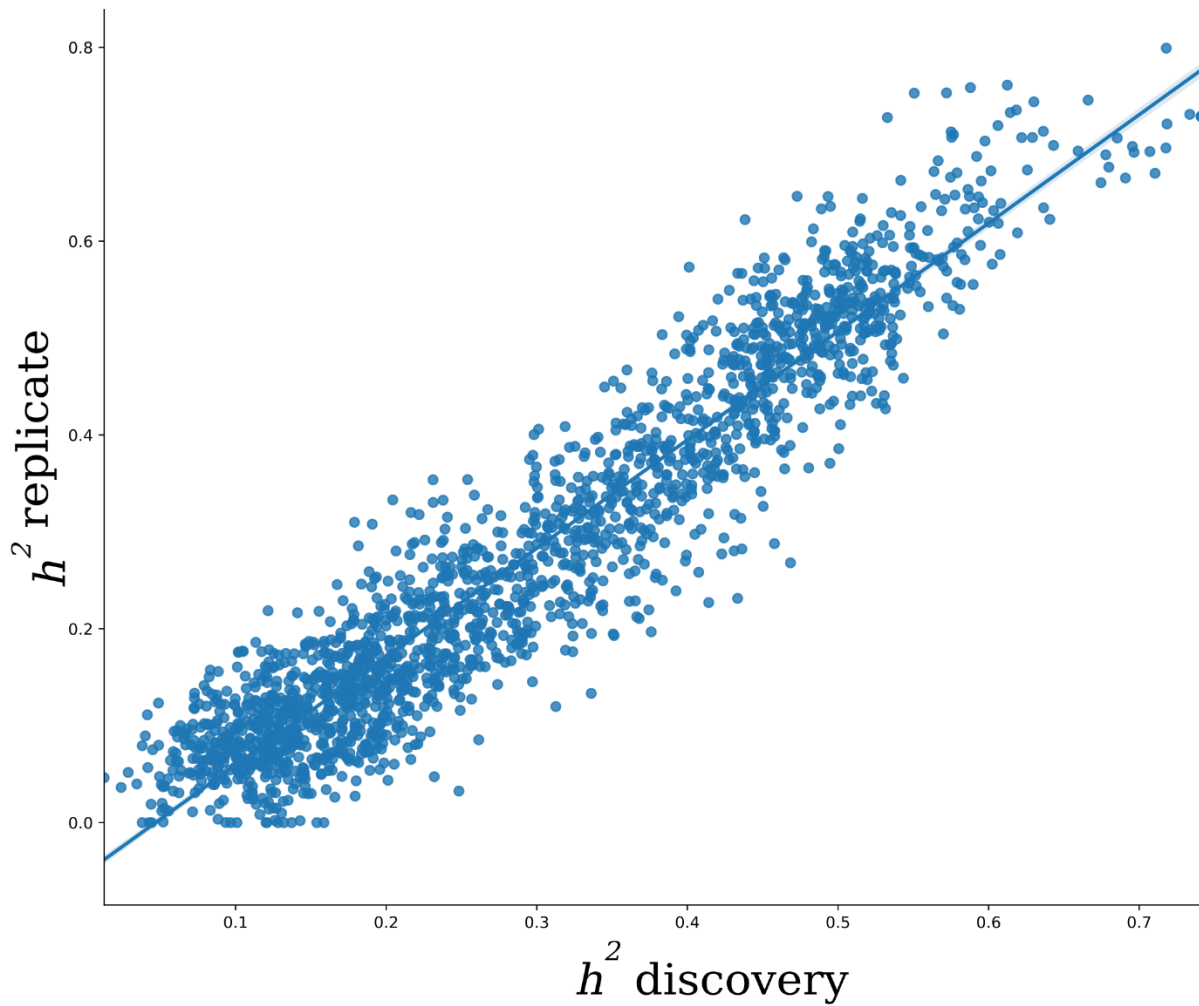


236  
237  
238  
239  
240  
241  
242  
243

**eFigure 1: Comparison between opNMF and sopNMF.** (A) Qualitative evaluation: The extracted components are shown in the original image space, with each PSC displayed in a distinct color. The white ellipse indicates the region where the models diverge. Quantitative evaluation: training loss (B, D) and sparsity (C, E) demonstrated similar patterns between models, except that batch size (BS) = 32 had a larger loss than the other models. Comparing the estimated memory consumption during training across models shows significant advantages for all sopNMF models compared to opNMF.

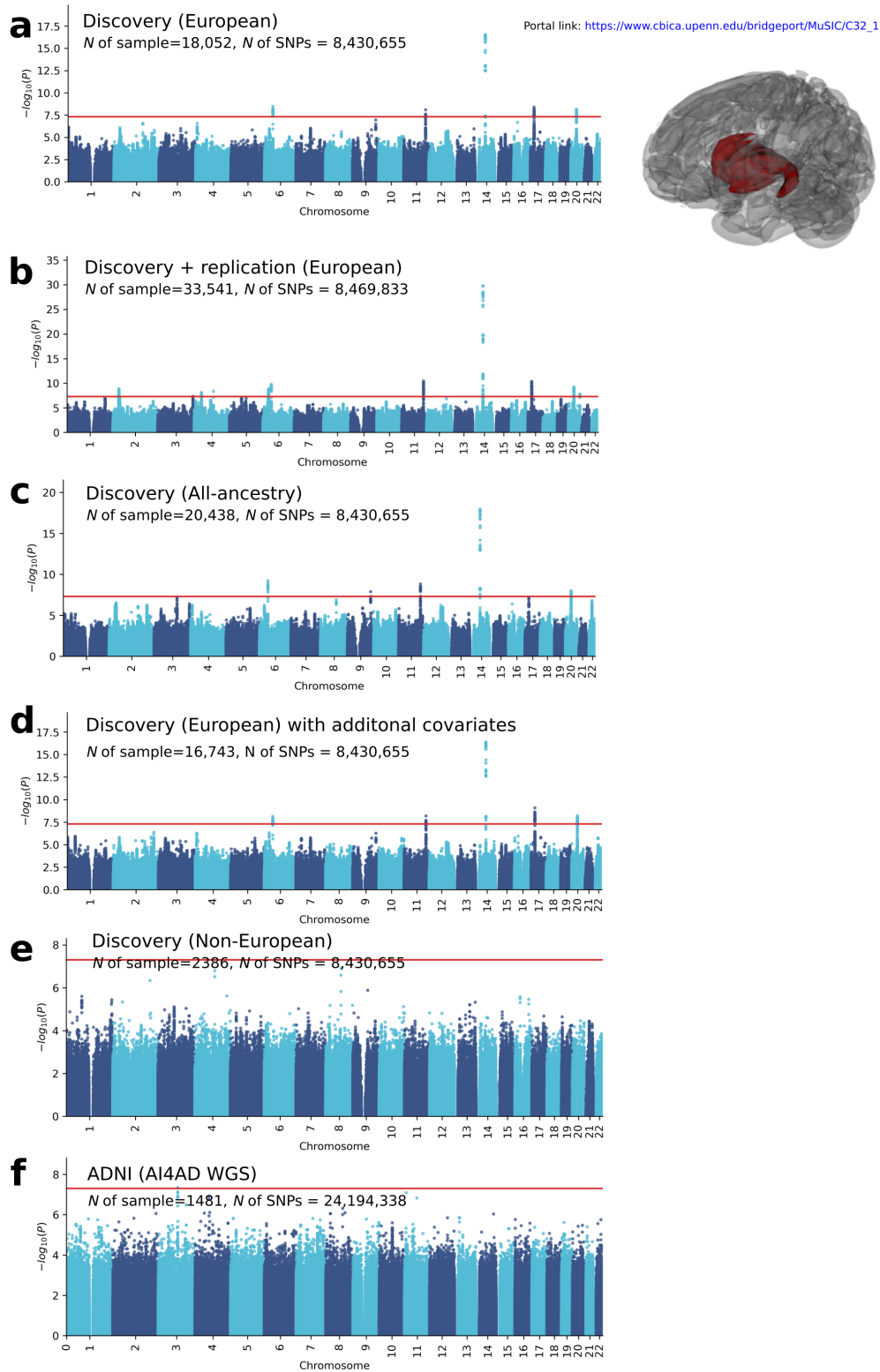


244  
 245 **eFigure 2: Reproducibility of the sopNMF brain parcellation.** In general, sopNMF  
 246 demonstrated high reproducibility under various conditions. For each brain PSC, the  
 247 reproducibility index (RI) was calculated (**Supplementary eMethod 2**). (A) Split-sample  
 248 analyses, where the training population ( $N=4000$ ) was randomly split into two halves while  
 249 maintaining similar age, sex, and site distribution between groups. (B) Split-sex  
 250 analyses, where the training population was divided into males and females. Colored PSCs on the brain template  
 251 illustrate the same PSC independently derived from the two splits. (C) Leave-one-site-out  
 252 analyses for C32 PSCs., where the training populations excluding participants from each site  
 253 (BIOCARD, ADNI, WARP, AIBL, ABIDE, BLSA, OASIS, CARDIA, PHENOM, PENN,  
 254 UKBB, and WHIMS) were independently trained with sopNMF. The RI indices were compared  
 255 to the sopNMF results using the full training sample ( $N=4000$ ).  
 256



258  
259  
260  
261  
262  
263  
264

**Figure 3: Scatter plot for the  $h^2$  estimates from the discovery and replication sets.** The SNP-based heritability was estimated independently for the discovery set ( $N=18,052$ ) and replication set ( $N=15,243$ ). In particular, the two estimates were highly correlated ( $r = 0.94$ ,  $p$ -value  $< 10^{-6}$ ), demonstrating a highly similar genetic architecture across different sets of UKBB data.

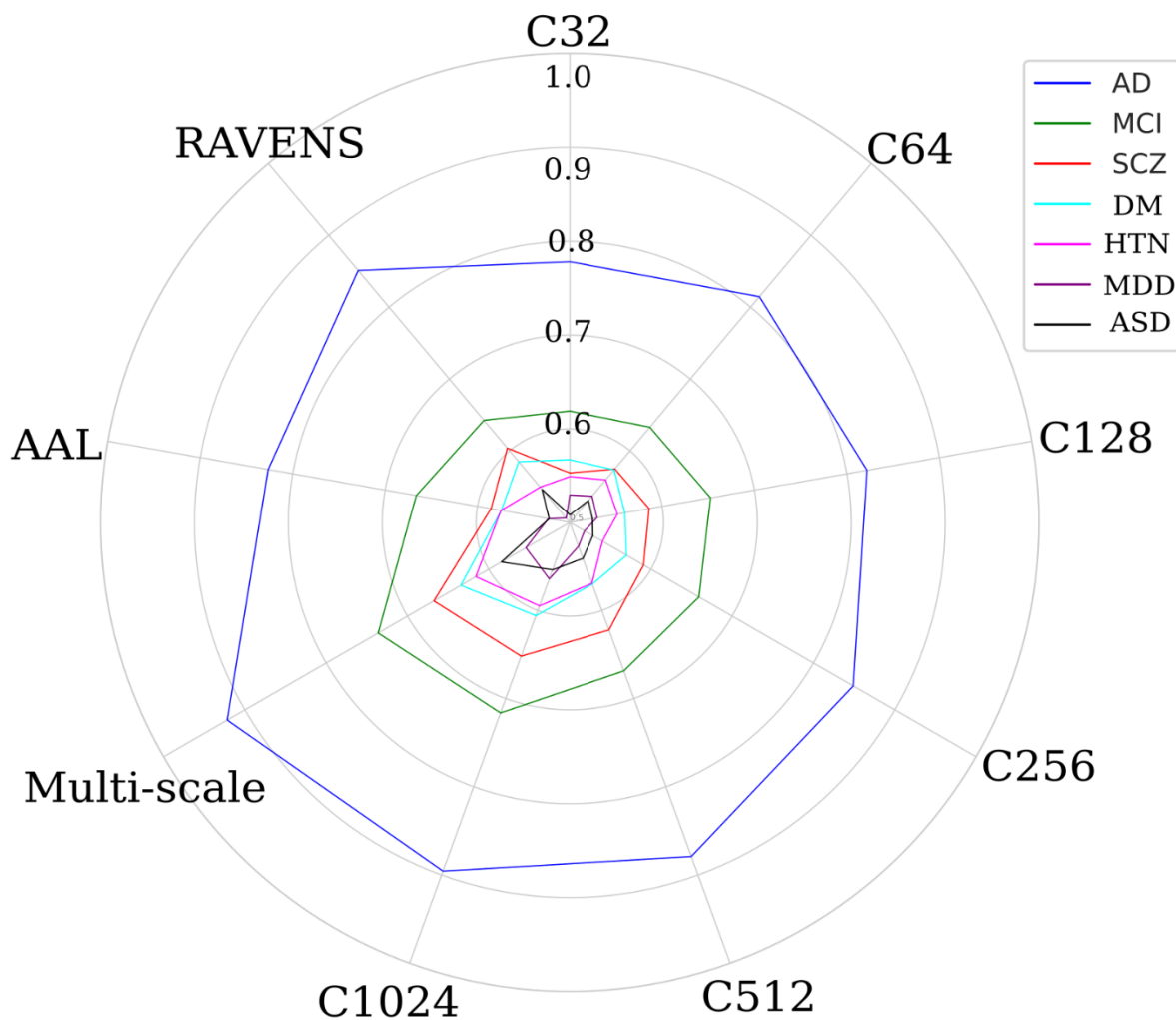


265  
266  
267  
268  
269

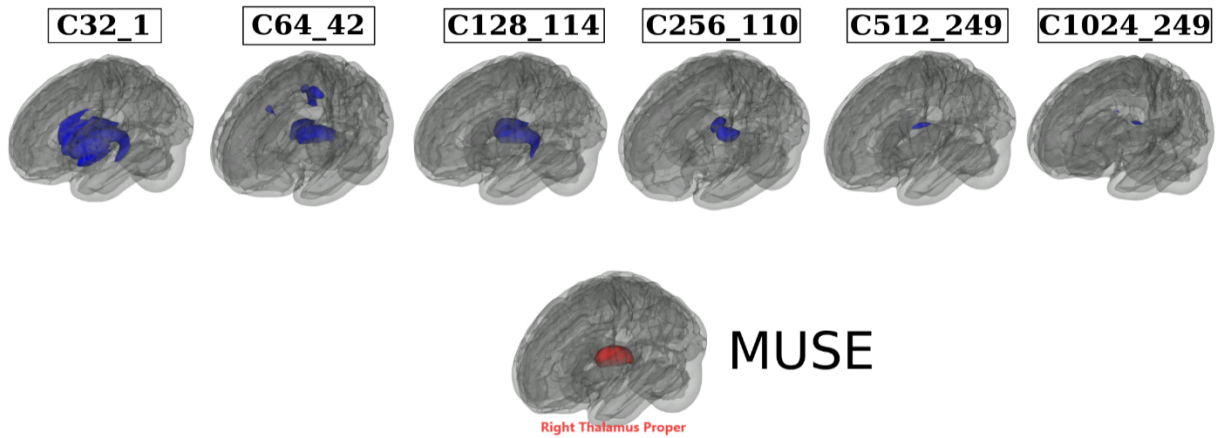
**eFigure 4: Sensitivity check for the GWAS results using the discovery set in UKBB.** **A)** The GWAS results for participants with European ancestry in the discovery set. **B)** The GWAS results for participants with European ancestry in the discovery and replication sets. **C)** The GWAS results for participants with all different ancestries in the discovery set. **D)** The GWAS



270 results for participants with European ancestry in the discovery set by adding four additional  
271 imaging-related covariates. **E)** The GWAS results for participants with non-European ancestry in  
272 the discovery set. **F)** The GWAS results for participants with the independent ADNI WGS data.



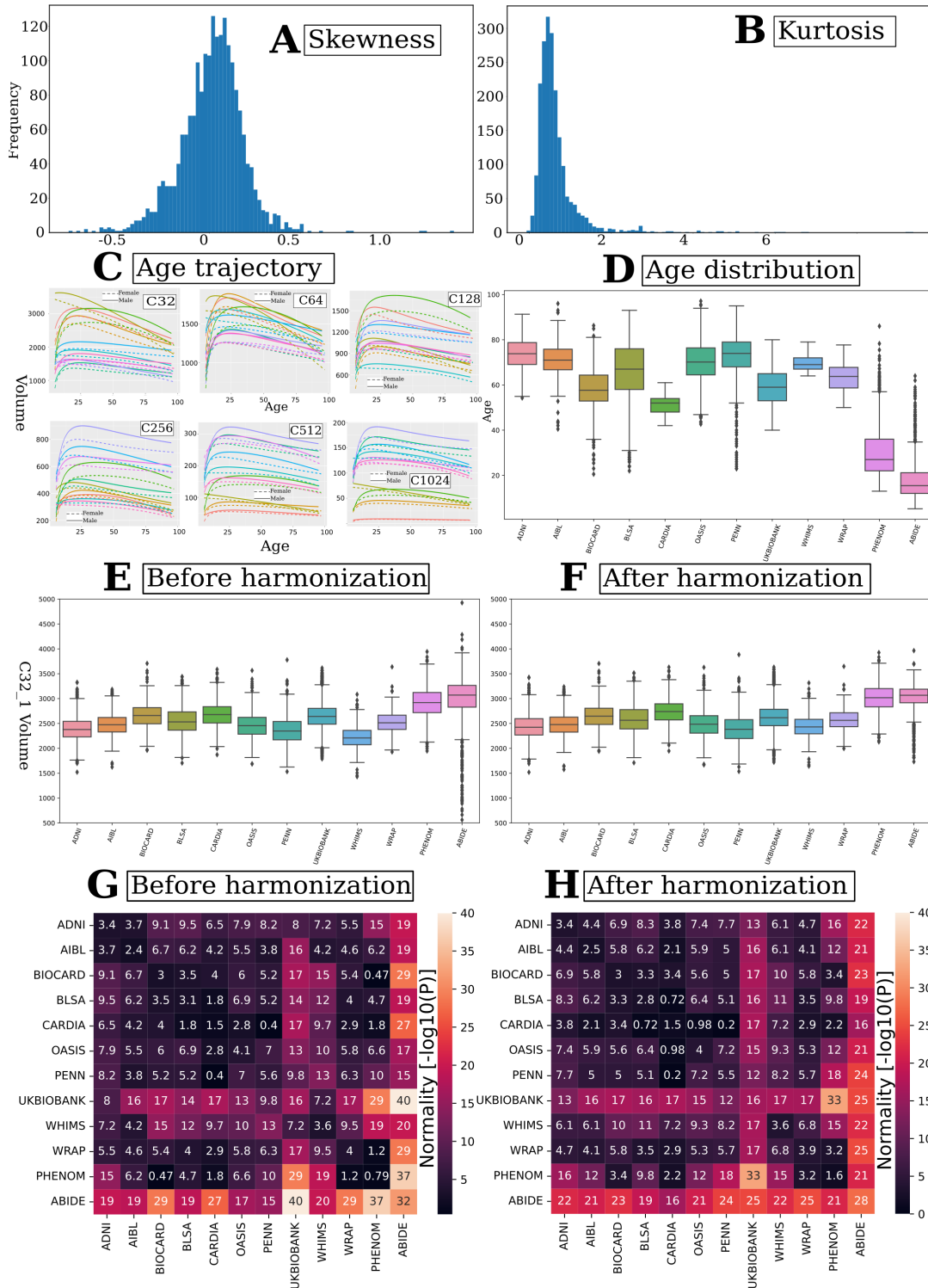
273  
 274 **eFigure 5: Machine learning performance for disease classification.** Balanced accuracy (BA)  
 275 for each classification task using different features from multi-scale MuSIC, AAL, and RAVENS  
 276 (higher score better). Details are presented in **eTable 4**.  
 277



278  
 279  
 280  
 281  
 282  
 283  
 284  
 285  
 286  
 287  
 288  
 289

**eFigure 6: Annotation of MUSE ROIs to MuSIC PSCs based on the overlap index.** We automatically annotated the 119 MUSE GM PSCs to the MuSIC atlases at all six scales ( $C=32, 64, 128, 256, 512,$  and  $1024$ ). To this end, we calculated an overlap index (OI) to quantify the spatial overlaps between MUSE and MuSIC. For instance, for each MUSE PSC (**eTable 5**) vs. each of the 32 PSCs of MuSIC at  $C=32$  scale, the OI equals the proportion of the number of overlap voxels and the total number of voxels in the MUSE PSC. Here we illustrate by mapping the right thalamus of MUSE to all 6 MuSIC atlases. The highest OIs are 0.82, 0.70, 0.86, 0.30, 0.09, 0.05 for C32\_1, C64\_42, C128\_114, C256\_110, C512\_249, and C1024\_249 PSCs. This functionality is available in BRIDGEPORT:

<https://www.cbica.upenn.edu/bridgeport/MUSE/Right%20Thalamus%20Proper>



290  
 291 **eFigure 7: Summary statistics of the multi-scale PSCs of MuSIC.** Multi-scale PSCs show  
 292 considerable normal distributions, i.e., symmetrical distribution (A) with a low kurtosis (B).  
 293 Moreover, we fit the Generalized Additive Model for Location, Scale, and Shape (GAMLSS)<sup>9</sup>  
 294 model (fractional polynomials with 2 degrees) to each PSC to delineate the age trajectory over  
 295 the lifespan in males (solid lines) and females (dotted lines), respectively (C). For visualization

296 purposes, we selectively display the first 10 PSCs from each scale of the MuSIC atlases. In  
297 general, males have larger brain volumes than females. For **D-F**, we selectively showed the  
298 distribution of age (**D**) and the distribution of PSC volume before harmonization (**E**) and after  
299 harmonization (**F**) for C32\_1 within each site in the discovery set. For **G** and **H**, we tested the  
300 normality of the PSC volume (C32\_1) from each pair of sites using the Shapiro-Wilk test  
301 (*scipy.stats.shapiro* function) in the discovery set before (**G**) harmonization and after  
302 harmonization (**H**). A higher  $-\log_{10}(P)$  indicates the data are less likely to be normally  
303 distributed. As a general trend, our statistical harmonization techniques demonstrated a slight  
304 improvement in the normality of the data. Additionally, we consistently applied normality  
305 transformations to all statistical analyses, including GWAS, to mitigate any non-normality.  
306

307 **eTable 1. Study cohort characteristics.**

308 The current study consists of two main populations/sets: the discovery set ( $N=32,440$ , including  
 309 participants from the first download of the UKBB data) and the replication set ( $N=18,259$ , the  
 310 second download of the UKBB data). To train the sopNMF model for MuSIC, we selected 250  
 311 patients (PT) and 250 healthy controls (CN) for each decade of the discovery set, resulting in  
 312 4000 participants in total, referred to as the training population. Age ranges from 5 to 97 years  
 313 and is shown with mean and standard deviation. Sex is displayed with the number and  
 314 percentage of female participants. Data was collected from 12 studies, 130 sites, and 12  
 315 countries. The number of sites (country) per study is detailed as follows:

- 316 • ADNI: 63 sites (USA)
- 317 • UKBB: 5 sites (UK)
- 318 • AIBL: 2 sites (Australia)
- 319 • BIOCARD: 2 sites (USA)
- 320 • BLSA: 1 site (USA)
- 321 • CARDIA: 3 sites (USA)
- 322 • OASIS: 1 site (USA)
- 323 • PENN: 1 site (USA)
- 324 • WHIMS: 14 sites (USA)
- 325 • WRAP 1 site (USA)
- 326 • PHENOM: 12 sites (China, Brazil, Australia, Germany, Spain, USA, Netherlands)
- 327 • ABIDE: 25 sites (USA, Netherlands, Belgium, Germany, Ireland, Switzerland, France)

328 Abbreviations: CN: healthy control; AD: Alzheimer's disease; MCI: mild cognitive impairment;  
 329 SCZ: schizophrenia; ASD: autism spectrum disorder; MDD: major depressive disorder; DM:  
 330 diabetes; HTN: hypertension.

331 <sup>a</sup>UKBB data were separately downloaded two times: the first was the  $N=21,305$  in the discovery  
 332 set, and the second was the replication set.

333 <sup>b</sup>We define CN (healthy controls) as participants that do not have any of the diseases listed here.  
 334 These CN participants might have diagnoses of other illnesses or comorbidities (e.g., participants  
 335 from UKBB have a wide range of pathology based on ICD-10).

336

Study	$N$ (50,699)	Age (5-97 year)	Sex (female/% )	CN <sup>b</sup>	AD	MCI	SCZ	ASD	MDD	DM	HTN
<b>Discovery set</b>	32,440	60.04± 14.87	16,868/52	24,980	954	1288	1094	597	1476	1093	958
ADNI	1765	73.66± 7.19	798/45	297	343	875	NA	NA	NA	NA	250
UKBB <sup>a</sup>	21,305	62.58± 7.48	10,101/53	18,735	1	NA	NA	NA	1476	1093	NA
AIBL	830	71.36± 6.78	471/57	625	86	115	NA	NA	NA	NA	4
BIOCARD	288	58.15± 10.54	115/60	283	1	4	NA	NA	NA	NA	NA
BLSA	1114	65.44± 14.11	589/53	729	9	11	NA	NA	NA	NA	365
CARDIA	892	51.21± 3.98	471/53	620	NA	NA	NA	NA	NA	NA	272
OASIS	983	69.92± 9.75	557/57	759	220	NA	NA	NA	NA	NA	4

PENN	807	72.63± 10.65	333/59	173	294	283	NA	NA	NA	NA	57
WHIMS	995	69.61± 3.64	995/100	986	NA	NA	NA	NA	NA	NA	6
WRAP	116	63.36± 6.06	79/68	116	NA	NA	NA	NA	NA	NA	NA
PHENOM	2125	30.21± 10.60	854/40	1031	NA	NA	1094	NA	NA	NA	NA
ABIDE	1220	17.92± 9.01	203/17	623	NA	NA	NA	597	NA	NA	NA
<b>Replication set<sup>a</sup></b>	18,259	54.70± 7.43	9742/53	NA	NA	NA	NA	NA	NA	NA	NA

337  
338

339 **eTable 2: Clinical phenotypes and diagnoses used in machine learning classification.**

340 We harmonized the population of the phenotypes of interest per study definitions:

- 341 • We combined AD and MCI patients from ADNI, PENN, and AIBL but excluded OASIS  
 342 subjects because of the different diagnostic criteria of an AD patient in OASIS.  
 343 • For several binary disease phenotypes, we used the ICD-10 diagnosis  
 344 (<https://biobank.ndph.ox.ac.uk/ukb/field.cgi?id=41270>). Note that ICD-10 diagnoses are  
 345 generally collected from the participants' medical inpatient records. We first included  
 346 diseases from the following categories:
- 347 ○ Diseases of the blood and blood-forming organs and certain disorders involving the
  - 348 immune mechanism (D-XXX, XXX represents the ID of a specific disease);
  - 349 ○ Endocrine, nutritional, and metabolic diseases (E-XXX);
  - 350 ○ Mental and behavioral disorders (F-XXX);
  - 351 ○ Diseases of the nervous system (G-XXX);
  - 352 ○ Diseases of the circulatory system (I-XXX).

353 We then set a threshold of 75 patients for any ICD-10 diagnosis. We finally randomly  
 354 selected age and sex-matched healthy controls (excluding all patients in all diagnoses). <sup>a</sup>:  
 355 For major depressive disorder, we used the inclusion criteria from our previous work.<sup>10</sup>

- 356 • For cognitive scores, we included:
- 357 ○ Tower rearranging (<https://biobank.ndph.ox.ac.uk/showcase/field.cgi?id=21004>)
  - 358 ○ Matrix pattern (<https://biobank.ndph.ox.ac.uk/showcase/field.cgi?id=6373>)
  - 359 ○ TMT-A (<https://biobank.ndph.ox.ac.uk/showcase/field.cgi?id=6348>)
  - 360 ○ TMT-B (<https://biobank.ndph.ox.ac.uk/showcase/field.cgi?id=6350>)
  - 361 ○ DSST (<https://biobank.ndph.ox.ac.uk/showcase/field.cgi?id=23324>)
  - 362 ○ Pairs matching (<https://biobank.ndph.ox.ac.uk/showcase/field.cgi?id=399>)
  - 363 ○ Numerical memory (<https://biobank.ndph.ox.ac.uk/showcase/field.cgi?id=4282>)
  - 364 ○ Prospective memory (<https://biobank.ndph.ox.ac.uk/showcase/field.cgi?id=4288>)
  - 365 ○ Reaction time (<https://biobank.ndph.ox.ac.uk/showcase/field.cgi?id=20023>)
  - 366 ○ Fluid intelligence (<https://biobank.ndph.ox.ac.uk/showcase/field.cgi?id=20016>)

367 AD: Alzheimer's disease; MCI: mild cognitive impairment; SCZ: schizophrenia; DM: diabetes  
 368 mellitus; MDD: major depressive disorder; HTN: hypertension; ASD: autism spectrum disorder;  
 369 CN: healthy control; PT: patient; *N*: number of participants. We decided not to harmonize  
 370 cognitive scores from different studies.

371

Trait (ICD-10 code or ID)	Sample size (CN/PT or <i>N</i> )	Site	Trait (ICD-10 code or ID)	Sample size (CN/PT or <i>N</i> )	Site
AD	1095/723	ADNI, PENN, & AIBL	Carpal tunnel syndrome (G560)	901/901	UKBB
MCI	1273/1095	ADNI, PENN, & AIBL	Lesion of ulnar nerve (G562)	104/104	UKBB
SCZ	1031/1094	PHENOM	Lesion of plantar nerve (G576)	163/163	UKBB
DM	1093/1093	UKBB	Angina pectoris (I20)	1535/1535	UKBB
MDD <sup>a</sup>	1476/1476	UKBB	Acute myocardial infarction (I21)	769/769	UKBB
HTN	934/887	ADNI, BLSA & CARDIA	Chronic ischaemic heart disease (I25)	2217/2217	UKBB



ASD	623/597	ABIDE	Pulmonary embolism (I20)	351/351	UKBB
Iron deficiency anemia (D50)	1012/1012	UKBB	Cardiomyopathy (I42)	116/116	UKBB
Vitamin B12 deficiency anemia (D50)	78/78	UKBB	Paroxysmal tachycardia (I47)	320/320	UKBB
Agranulocytosis (D70)	245/245	UKBB	Heart failure (I50)	436/436	UKBB
Thyrotoxicosis (E05)	205/205	UKBB	Cerebral infarction (I63)	291/291	UKBB
Vitamin D deficiency (E55)	180/180	UKBB	Vitamin B deficiency (E53)	130/130	UKBB
Obesity (E66)	1481/1481	UKBB	Hemiplegia (G81)	111/111	UKBB
Lipoprotein metabolism disorder (E78)	3880/3880	UKBB	Facial nerve disorders (G51)	95/95	UKBB
Mineral metabolism disorder (E83)	291/291	UKBB	Tower rearranging (21004)	8412	UKBB
Volume depletion	240/240	UKBB	Matrix pattern (6373)	8501	UKBB
Delirium	92/92	UKBB	TMT-A (6348)	8599	UKBB
Alcohol abuse	341/341	UKBB	TMT-B (6350)	8599	UKBB
Tobacco abuse	863/863	UKBB	DSST (23324)	8523	UKBB
Bipolar affective disorder	77/77	UKBB	Pairs matching (399)	20945	UKBB
Phobic anxiety disorder	84/84	UKBB	Numerical memory (4282)	9323	UKBB
Multiple sclerosis	109/109	UKBB	Prospective memory (4288)	19681	UKBB
Epilepsy	250/250	UKBB	Reaction time (20023)	21258	UKBB
Migraine	508/508	UKBB	Fluid intelligence (20016)	19184	UKBB
Sleep disorders	590/590	UKBB			

372  
373

374 **eTable 3: Comparison of variants identified via MuSIC with other studies.** Using the AAL  
375 atlas, we found (using the same data in the current study) that 269 independent significant SNPs  
376 had 356 pairwise associations with 54 AAL brain regions. 230 out of the 269 SNPs matched with  
377 the SNPs in MuSIC. Among the 39 unmatched SNPs, 15 SNPs were in linkage disequilibrium  
378 (LD,  $r^2 > 0.6$ ) with MuSIC SNPs (**Supplementary eFile 5**). As a second example, Zhao et al.<sup>11</sup>  
379 reported that 251 independent significant SNPs had 346 pairwise associations with 43 GM regions  
380 using the Mindboggle atlas on the UKBB ( $N=19,629$ ).<sup>12</sup> 129 of the 251 SNPs matched with SNPs  
381 identified by MuSIC. Among these non-matching SNPs (127), 31 were in LD with MuSIC SNPs  
382 (**Supplementary eFile 6**). Similarly, Elliot et al.<sup>13</sup> ( $N=8428$ ) discovered that 20 independent  
383 significant SNPs had 58 pairwise associations with 52 GM regions from atlases in Freesurfer and  
384 FSL software. Out of the 20 SNPs, 16 coincided with MuSIC SNPs. Among the four unmatched  
385 SNPs, 1 SNP was in LD with MuSIC SNPs (**Supplementary eFile 7**). Note that the definition of  
386 independent significant SNPs or genomic loci might slightly differ between studies.

Study/Atlas	Identified genomic loci	Matched loci	Loci in LD	Novel loci	Database	Sample size	Ancestry
MuSIC	915	NA	NA	NA	UKBB	18,052	European
AAL	218	162	13	740	UKBB	18,052	European
Zhao et al. <sup>11</sup>	251	73	14	828	UKBB	19,629	European
Elliot et al. <sup>13</sup>	20	16	1	898	UKBB	8428	European
GWAS Catalog	NA	298	NA	617	NA	NA	NA

387  
388

389 **eTable 4: Classification balanced accuracy for disease classification and effect size of these**  
 390 **imaging signatures.**

391 Disease classification performance is presented using balanced accuracy. The mean and standard  
 392 deviation are presented. Cohen's  $d$  was computed to compare the SPARE scores between groups.  
 393 Multi-scale classification<sup>a</sup>: All 2003 PSCs from multiple scales were fit into the classifier.  
 394 Multi-scale classification<sup>b</sup>: PSCs from all scales were fit into the classifier with a nested feature  
 395 selection procedure (SVM-REF). The motivation is that PSCs from different scales are  
 396 hierarchical and correlated. The nested feature selection can select the features most relevant to  
 397 the specific task. We avoided any statistical comparison of the performance of machine learning  
 398 models because available statistical tests are liberal and often lead to false-positive conclusions  
 399 due to the complexity of the cross-validation procedure.<sup>14</sup>

400 a): Classification results for all subjects in all sites using a nested CV procedure

PSC	AD	$d$	MCI	$d$	SCZ	$d$	DM	$d$	HTN	$d$	MDD	$d$	ASD	$d$
C32	0.78± 0.02	1.52	0.62± 0.02	0.59	0.55± 0.02	0.30	0.56± 0.02	0.35	0.55± 0.02	0.28	0.52± 0.02	0.16	0.50± 0.02	0.07
C64	0.81± 0.02	1.73	0.63± 0.02	0.66	0.57± 0.02	0.41	0.57± 0.02	0.40	0.56± 0.02	0.31	0.53± 0.02	0.17	0.53± 0.02	0.19
C128	0.82± 0.02	1.82	0.65± 0.02	0.76	0.59± 0.02	0.47	0.56± 0.02	0.33	0.55± 0.02	0.30	0.52± 0.02	0.15	0.52± 0.02	0.15
C256	0.85± 0.02	2.08	0.66± 0.02	0.91	0.59± 0.02	0.50	0.56± 0.02	0.47	0.54± 0.02	0.31	0.51± 0.02	0.13	0.52± 0.02	0.16
C512	0.88± 0.02	2.34	0.67± 0.02	1.06	0.62± 0.02	0.62	0.57± 0.02	0.54	0.56± 0.02	0.42	0.52± 0.02	0.05	0.54± 0.02	0.24
C1024	0.90± 0.02	2.50	0.72± 0.02	1.12	0.65± 0.02	0.75	0.60± 0.02	0.59	0.59± 0.02	0.46	0.56± 0.02	0.13	0.55± 0.02	0.29
Multi-scale <sup>a</sup>	0.91± 0.02	2.54	0.72± 0.02	1.12	0.66± 0.02	0.77	0.61± 0.02	0.64	0.59± 0.02	0.47	0.55± 0.02	0.23	0.56± 0.02	0.30
Multi-scale <sup>b</sup>	0.92± 0.02	2.61	0.73± 0.02	1.13	0.67± 0.02	0.78	0.64± 0.02	0.67	0.61± 0.02	0.49	0.55± 0.02	0.26	0.58± 0.02	0.32
AAL	0.82± 0.02	1.81	0.66 ±0.02	0.75	0.59± 0.02	0.46	0.57± 0.02	0.32	0.57± 0.02	0.35	0.52± 0.02	0.08	0.52± 0.02	0.14
RAVENS	0.85± 0.02	2.04	0.64 ±0.02	0.74	0.60± 0.02	0.45	0.58± 0.02	0.33	0.55± 0.02	0.34	0.50± 0.02	0.05	0.54± 0.02	0.15

401 b): The classification results of the balanced accuracy (BA) from the test data in the nested CV  
 402 and the independently left-out site for the task of AD vs. CN were assessed using all available  
 403 multi-scale PSCs<sup>a</sup>. Three sites, namely ADNI, AIBL, and PENN, were considered for this  
 404 analysis. However, UKBB, BIOCARD, and BLSA data were excluded due to limited AD cases  
 405 (**eTable 1**). Similarly, data from OASIS were excluded due to discrepancies in the diagnosis  
 406 criteria for AD, as previously stated in our previous work<sup>7</sup>.

Left-out site	Test BA in CV	Test BA in the left-out site
ADNI	0.90±0.02	0.88±0.02
AIBL	0.88±0.02	0.95±0.02
PENN	0.90±0.02	0.95±0.02

408

409  
410

**eTable 5:** 119 MUSE gray matter regions of interest.  
L: Left hemisphere; R: Right hemisphere; ROI: region of interest.

MUSE ROI	MUSE ROI	MUSE ROI
Precentral gyrus (R)	Occipital fusiform gyrus (R)	Anterior insula (L)
Precentral gyrus (L)	Planum temporale (R)	Anterior orbital gyrus (R)
Accumbens area (R)	Cerebellar vermal lobules I-V	Anterior orbital gyrus (L)
Accumbens area (L)	Cerebellar vermal lobules VI-VII	Angular gyrus (R)
Amygdala (R)	Cerebellar vermal lobules VIII-X	Angular gyrus (L)
Amygdala (L)	Basal forebrain (R)	Calcarine cortex (R)
Occipital pole (L)	Basal forebrain (L)	Calcarine cortex (L)
Caudate (R)	Middle temporal gyrus (L)	Central operculum (R)
Caudate (L)	Occipital pole (R)	Central operculum (L)
Cerebellum exterior (R)	Planum temporale (L)	Cuneus (R)
Cerebellum exterior (L)	Parietal operculum (L)	Cuneus (L)
Planum polare (L)	Postcentral gyrus (R)	Entorhinal area (R)
Middle temporal gyrus (R)	Postcentral gyrus (L)	Entorhinal area (L)
Hippocampus (R)	Posterior orbital gyrus (R)	Frontal operculum (R)
Hippocampus (L)	Temporal pole (R)	Frontal operculum (L)
Precentral gyrus medial segment (R)	Temporal pole (L)	Frontal pole (R)
Precentral gyrus medial segment (L)	Triangular part of the inferior frontal gyrus (R)	Frontal pole (L)
Superior frontal gyrus medial segment (R)	Triangular part of the inferior frontal gyrus (L)	Fusiform gyrus (R)
Superior frontal gyrus medial segment (L)	Transverse temporal gyrus (R)	Fusiform gyrus (L)
Pallidum (R)	Superior frontal gyrus medial segment (L)	Gyrus rectus (R)
Pallidum (L)	Planum polare (R)	Gyrus rectus (L)
Putamen (R)	Transverse temporal gyrus (L)	Inferior occipital gyrus (R)
Putamen (L)	Anterior cingulate gyrus (R)	Inferior occipital gyrus (L)
Thalamus proper (R)	Anterior cingulate gyrus (L)	Inferior temporal gyrus (R)
Thalamus proper (L)	Anterior insula (R)	Inferior temporal gyrus (L)
Lingual gyrus (R)	Occipital fusiform gyrus (L)	Subcallosal area (R)
Lingual gyrus (L)	Opercular part of inferior frontal gyrus (R)	Subcallosal area (L)
Lateral orbital gyrus (R)	Opercular part of inferior frontal gyrus (L)	Superior frontal gyrus (R)
Lateral orbital gyrus (L)	Orbital part of inferior frontal gyrus (R)	Superior frontal gyrus (L)
Middle cingulate gyrus (R)	Orbital part of inferior frontal gyrus (L)	Supplementary motor cortex (R)
Middle cingulate gyrus (L)	Posterior cingulate gyrus (R)	Supplementary motor cortex (L)
Medial frontal cortex (R)	Posterior cingulate gyrus (L)	Supramarginal gyrus (R)
Medial frontal cortex (L)	Precuneus (R)	Supramarginal gyrus (L)
Middle frontal gyrus (R)	Precuneus (L)	Superior occipital gyrus (R)
Middle frontal gyrus (L)	Parahippocampal gyrus (R)	Superior occipital gyrus (L)
Middle occipital gyrus (R)	Parahippocampal gyrus (L)	Superior parietal lobule (R)
Middle occipital gyrus (L)	Posterior insula (R)	Superior parietal lobule (L)
Medial orbital gyrus (R)	Posterior insula (L)	Superior temporal gyrus (R)
Medial orbital gyrus (L)	Parietal operculum (R)	Superior temporal gyrus (L)
Superior frontal gyrus medial segment (R)	Posterior orbital gyrus (L)	

411

412 **eAlgorithm 1:** Algorithm for sopNMF.  
 413 The source code of the Python implementation of sopNMF is available here:  
 414 <https://github.com/anbai106/SOPNMF>

---

**Algorithm 1:** sopNMF

---

- **Input:** maximum number of epochs  $e$ , number of component  $C$  or  $r$ , batch size  $b$ , early stopping criteria  $\theta$  (i.e., the loss without decreasing for a certain epochs) ;
- **Output:**  $\mathbf{W} \in \mathbb{R}^{d \times r}$ ,  $\mathbf{H} \in \mathbb{R}^{r \times n}$  ;
- **Initialization:**  $\mathbf{W}$  ;

```

if not  $\theta$  or epoch  $\neq e$  then
  for  $p \leftarrow 0$  to  $e$  do
    for  $i \leftarrow 0$  to  $t$  do
      Read mini-batch  $\mathbf{X}_{bi}$ 
      Update  $\mathbf{W}_{i+1}$  via Eq. 2
    end
     $loss = \sum_{i=1}^{\lfloor \frac{n}{b} \rfloor} \|\mathbf{X}_{bi} - \mathbf{W}\mathbf{W}^T \mathbf{X}_{bi}\|_F^2$  (Eq.3)
    if loss in  $\theta$  then
      Stop
    else
      Shuffle  $\mathbf{X}$ 
      Continue
    end
  end
else
  Stop
end

```

---

415  
 416  
 417

418 **References**

- 419
- 420 1. Shalev-Shwartz, S., Singer, Y. & Ng, A. Y. Online and batch learning of pseudo-metrics. in
- 421 *Proceedings of the twenty-first international conference on Machine learning* 94
- 422 (Association for Computing Machinery, 2004). doi:10.1145/1015330.1015376.
- 423 2. Kuhn, H. W. The Hungarian method for the assignment problem. *Naval Research Logistics*
- 424 *Quarterly* **2**, 83–97 (1955).
- 425 3. Pomponio, R. *et al.* Harmonization of large MRI datasets for the analysis of brain imaging
- 426 patterns throughout the lifespan. *Neuroimage* **208**, 116450 (2020).
- 427 4. Watanabe, K., Taskesen, E., van Bochoven, A. & Posthuma, D. Functional mapping and
- 428 annotation of genetic associations with FUMA. *Nat Commun* **8**, 1826 (2017).
- 429 5. Purcell, S. *et al.* PLINK: A Tool Set for Whole-Genome Association and Population-Based
- 430 Linkage Analyses. *Am J Hum Genet* **81**, 559–575 (2007).
- 431 6. Samper-González, J. *et al.* Reproducible evaluation of classification methods in
- 432 Alzheimer’s disease: Framework and application to MRI and PET data. *NeuroImage* **183**,
- 433 504–521 (2018).
- 434 7. Wen, J. *et al.* Convolutional neural networks for classification of Alzheimer’s disease:
- 435 Overview and reproducible evaluation. *Medical Image Analysis* **63**, 101694 (2020).
- 436 8. Wen, J. *et al.* Reproducible Evaluation of Diffusion MRI Features for Automatic
- 437 Classification of Patients with Alzheimer’s Disease. *Neuroinformatics* **19**, 57–78 (2021).
- 438 9. Stasinopoulos, D. M. & Rigby, R. A. Generalized Additive Models for Location Scale and
- 439 Shape (GAMLSS) in R. *Journal of Statistical Software* **23**, 1–46 (2008).

- 440 10. Wen, J. *et al.* Characterizing Heterogeneity in Neuroimaging, Cognition, Clinical  
441 Symptoms, and Genetics Among Patients With Late-Life Depression. *JAMA Psychiatry*  
442 (2022) doi:10.1001/jamapsychiatry.2022.0020.
- 443 11. Zhao, B. *et al.* Genome-wide association analysis of 19,629 individuals identifies variants  
444 influencing regional brain volumes and refines their genetic co-architecture with cognitive  
445 and mental health traits. *Nat Genet* **51**, 1637–1644 (2019).
- 446 12. Klein, A. & Tourville, J. 101 Labeled Brain Images and a Consistent Human Cortical  
447 Labeling Protocol. *Frontiers in Neuroscience* **6**, 171 (2012).
- 448 13. Elliott, L. T. *et al.* Genome-wide association studies of brain imaging phenotypes in UK  
449 Biobank. *Nature* **562**, 210–216 (2018).
- 450 14. Nadeau, C. & Bengio, Y. Inference for the Generalization Error. in *Advances in Neural*  
451 *Information Processing Systems 12* (eds. Solla, S. A., Leen, T. K. & Müller, K.) 307–313  
452 (MIT Press, 2000).
- 453